

## Investigations on double-state behavior of the counterflow premixed flame system

Viswanath R. Katta <sup>a,\*</sup>, Shengteng Hu <sup>b</sup>, Peiyong Wang <sup>b</sup>,  
Robert W. Pitz <sup>b</sup>, William M. Roquemore <sup>c</sup>, James R. Gord <sup>c</sup>

<sup>a</sup> *Innovative Scientific Solutions, Inc., 2766 Indian Ripple Road, Dayton, OH 45440, USA*

<sup>b</sup> *Mechanical Engineering Department, Vanderbilt University, Nashville, TN 37235, USA*

<sup>c</sup> *Propulsion Directorate, Air Force Research Laboratory, Wright Patterson Air Force Base, OH 45433, USA*

### Abstract

The counterflow flame system established between lean-methane–air and lean-hydrogen–air streams is investigated experimentally and numerically. A two-dimensional model known as UNICORN was used for the simulation. Detailed measurements for temperature and species concentrations were obtained along the centerline using Raman spectroscopy. A double-state behavior for this flame system was identified in the numerical simulations, which was later confirmed by the experiments. For the given flow conditions, the flame system can have either a single-flame or a double-flame structure depending on the way those conditions were achieved. Detailed comparisons were made between measurements and calculations for the two flame structures. Calculations for various lean methane–air mixtures and stretch rates were performed to understand the double-state behavior of counterflow premixed flames. It was found that the flame system exhibits double-state behavior only for leaner ( $\phi_{\text{CH}_4} < 0.74$ ) methane–air mixtures. Aerodynamic and chemical structures of the flames in different stretch-rate regimes were analyzed. When stretch rate on the flame system is increased, the flame transitions from a double-flame to a single-flame structure due to aerodynamic-cooling process. When stretch rate is decreased, the flame does not transition back to the double-flame structure due to stretch effects on molecular diffusion. However, for ( $\phi_{\text{CH}_4} > 0.81$ ), decrease in stretch rate increases flame temperature due to lack of stretch-induced cooling and returns the flame structure to a double-flame one. For a narrow range of equivalence ratios (0.74–0.81) counterflow premixed flames exhibit a hysteresis property.

© 2006 The Combustion Institute. Published by Elsevier Inc. All rights reserved.

*Keywords:* Premixed flames; Extinction; Stretch rate; Double states; Lean combustion

### 1. Introduction

Lean combustion is of interest due to its potential advantages in limiting thermal  $\text{NO}_x$  emissions and in increasing fuel consumption efficiency.

Typically, diluted fuel–air mixtures are obtained through either available excess air or exhaust-gas recirculation. Lean combustion has been used in gas turbines and direct injection spark ignition (DISI) engines. However, a critical problem in using lean combustion is that it tends to produce unburned hydrocarbon pollutants. For example, in DISI engines, ultra-lean combustion is achieved by charge stratification. The fuel/air mixture is

\* Corresponding author. Fax: +1 937 656 4110.  
E-mail address: [vrkatta@erinet.com](mailto:vrkatta@erinet.com) (V.R. Katta).

inhomogeneous, leading to the simultaneous formation of lean, rich and stoichiometric regions. For the inhomogeneous reactants, Haworth et al. [1] simulated turbulent inhomogeneous combustion in DISI engines and found that hydrocarbon-rich fragments and oxidizer penetrate behind the primary heat-release zone to form a secondary reaction zone and, thereby, pollutants. Flames occurring in an inhomogeneously mixed fuel and air regions are also examples of partially premixed combustion. Some of this partially premixed mixture is so lean that it does not burn. However, such ultra-lean mixtures may still combust if hot products interact with it. That is, under certain conditions, the lean mixture region can burn and thus reduce the potential pollutants. The focus of this work is to study interaction of lean mixture with hot products that are needed to maintain the lean region burning. Partially premixed flames have been studied widely. In particular, the downstream interaction of two premixed streams was investigated by Sohrab et al. [2]. On the other hand, most practical flames are stretched to different extents. The stretch effects combined with other aspects such as the effect of Lewis number or curvature will modify flame structure significantly [3,4]. Considering the various conditions that exist simultaneously in inhomogeneous fuel/air reaction, a set of  $\text{CH}_4$ /air flames with a wide range of equivalence ratios and stretch rates impinging upon counterflowing hot products are studied experimentally and numerically. The opposed jet burner that generates nearly flat flames are widely used to study chemical kinetics and species transport under aerodynamic stretch. Using the counterflow jet flames, partially premixed  $\text{CH}_4$ /air versus air flame structures were investigated [5,6]. Structures of the lean partially premixed  $\text{CH}_4$  and  $\text{C}_3\text{H}_8$  flames established between the fuels and the hot products have also been investigated [7–9]. In general, premixed flames [10,11] are much less sensitive to stretch than diffusion flames [12]. In the present work, stretch effects on the flame structure of lean  $\text{CH}_4$ /air mixtures are studied using a two-dimensional, detailed transport, complex chemistry numerical model.

## 2. Numerical model

A time-dependent, axisymmetric mathematical model known as UNICORN (Unsteady Ignition and Combustion using ReactionNs) [13,14] is used for the simulation of the unsteady counterflow premixed flames. It solves for axial- and radial-momentum equations, continuity, and enthalpy- and species-conservation equations on a staggered-grid system. A clustered mesh system is employed to trace the large gradients in flow variables near the flame surface. A detailed chemical-kinetics model (GRI Version 1.2) of Gas

Research Institute [15] is incorporated into UNICORN for the investigation of methane–hydrogen flames. It consists of 32 species and 346 elementary-reaction steps. Thermo-physical properties such as enthalpy, viscosity, thermal conductivity, and binary molecular diffusion of all the species are calculated from the polynomial curve fits developed for the temperature range 300–5000 K. Mixture viscosity and thermal conductivity are then estimated using the Wilke and Kee expressions, respectively. Molecular diffusion is assumed to be of the binary-diffusion type, and the diffusion velocity of a species is calculated using Fick's law and the effective-diffusion coefficient of that species in the mixture. A simple radiation model based on the optically thin-media assumption [16] is incorporated into the energy equation. Only radiation from  $\text{CH}_4$ ,  $\text{CO}$ ,  $\text{CO}_2$ , and  $\text{H}_2\text{O}$  is considered in the present study. Radiation from soot is not considered, which is justified for the nearly non-sooting lean premixed flames studied.

The finite-difference forms of the momentum equations are obtained using an implicit QUICK-EST scheme [17], and those of the species and energy equations are obtained using a hybrid scheme of upwind and central differencing. At every time step, the pressure field is accurately calculated by solving all the pressure Poisson equations simultaneously and using the LU (Lower and Upper diagonal) matrix-decomposition technique. The computational domain is bounded between sets of inflow boundaries in the axial direction and between the axis of symmetry and outflow boundaries in the radial direction. The boundary conditions are treated in the same way as that reported in earlier papers [17,18].

## 3. Experiment

The counterflow burner used in this study was designed by Seshadri et al. [19] which has been extensively considered for hydrogen- and hydrocarbon-fueled diffusion flames and for hydrocarbon-fueled premixed flames. With the honeycomb inserts, rather than wire screens, it has also been used for the studies of lean  $\text{H}_2$ /air premixed flames [20]. The schematic diagram of the burner along with the supplied flows is shown in Fig. 1. The burner system consists of 25-mm diameter inner nozzles that are separated by 12.6 mm. Methane–air mixture was issued from the top nozzle while hydrogen–air mixture was issued from the bottom nozzle. The honeycomb flow straighteners inserted in the flow supplies yielded uniform exit velocities [20]. A low-speed nitrogen flow was issued from the top and bottom outer nozzles for protecting the flame from the room-air disturbances. The exit temperature for all the gases was 300 K. Measurements of major

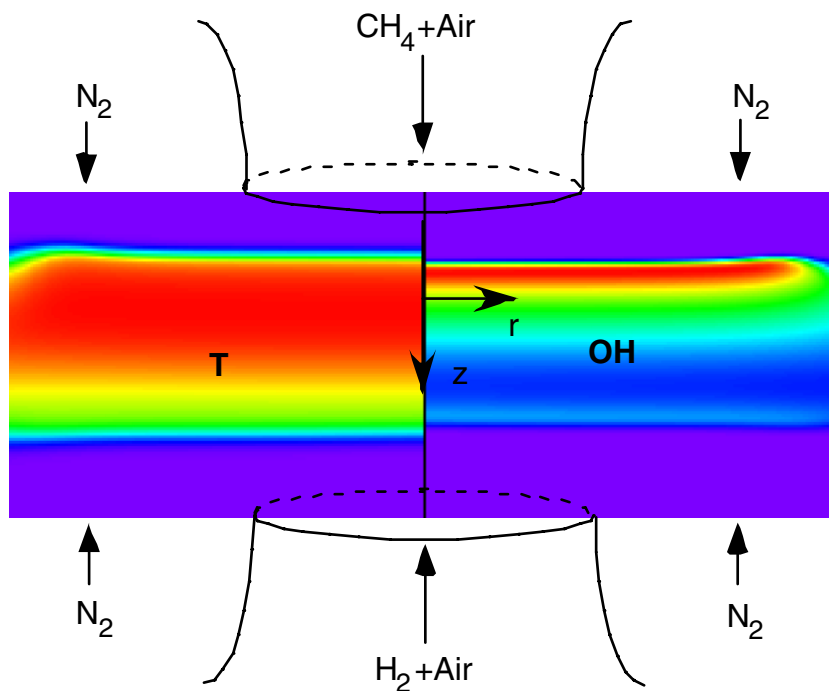


Fig. 1. Premixed flame system used for the investigation of products-supported lean combustion. Typical temperature and OH-concentration distributions are shown in the left and right halves, respectively.

species and temperature were made along the centerline using a non-intrusive, Raman-scattering diagnostic system [8,20]. Experiments were performed for various equivalence ratios and stretch rates. Details of eight flames that were classified into three groups are given in Ref. [20]. For example, Group A includes three flames with the same  $\text{CH}_4/\text{air}$  mixture (with an equivalence ratio of 0.68) and lean  $\text{H}_2/\text{air}$  mixture (with an equivalence ratio of 0.28) but subjected to different stretch rates [20]. In this study, two additional flames are measured with a slightly leaner  $\text{CH}_4$ -air mixture ( $\phi = 0.64$ ).

#### 4. Results and discussion

Two-dimensional calculations for the premixed flame system developed between the upper and lower nozzles were made using UNICORN code on a grid system that has  $421 \times 101$  node points in the axial ( $z$ ) and radial ( $r$ ) directions, respectively. Flat velocity profiles were used at the nozzle exits. Computed results in the form of temperature and OH-concentration distributions for a typical flame in Group A are shown in Fig. 1. The global stretch rate (defined as the ratio between twice the velocity difference and the nozzle separation) applied on this flame was  $90 \text{ s}^{-1}$ . Even though the computational domain was

extended to 20 mm in the radial direction, only the data up to 15 mm is shown in Fig. 1. Calculations have yielded a double-flame structure with methane flame (lower) burning more intensely than the hydrogen one (upper). Former flame is also shorter (in the radial direction) than the latter. Detailed comparisons made between the computed and measured temperature and species profiles along the centerline [21] suggested that UNICORN code with GRI-V1.2 chemical kinetics predicts the flame structure accurately.

Increasing the velocities of the hydrogen- and methane-fuel jets increases the applied stretch rate on the double-flame system and decreases the separation between the two flames. At a certain stretch rate, the methane flame extinguishes and the flame system switches from a double-flame structure to a single-flame one. Interestingly, significant differences developed between the predictions and measurements when the stretch rate was increased to  $204 \text{ s}^{-1}$ . While experiments produced a single flame, calculations have predicted a double-flame structure. Repeated calculations with different grid sizes and for stretch rates slightly higher and lower than  $204 \text{ s}^{-1}$  failed to predict the single-flame structure. Note that calculations made by Cheng et al. [20] using OPPDIF code also resulted in a double-flame structure for this stretch-rate condition. Their efforts in using different chemical kinetics models have also failed.

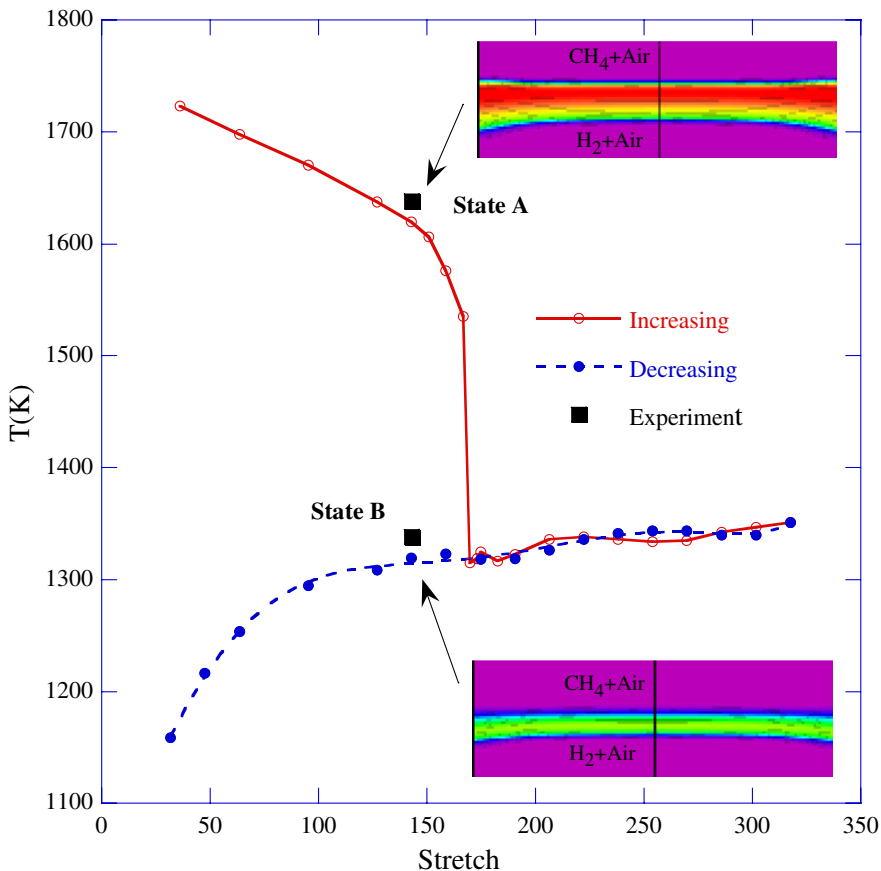


Fig. 2. Response of a premixed flame formed between counter-flowing methane–air and hydrogen–air jets to increasing (open circles) and decreasing (solid circles) strain rates.  $\Phi_{CH_4} = 0.64$ ,  $\Phi_{H_2} = 0.28$ . Insets show the temperature images of two stable states under identical conditions.

Additional calculations are performed for understanding the discrepancy between the predicted and measured flame structures for the  $204\text{-s}^{-1}$ -stretch-rate case. Typically, finite-rate chemistry calculations for a flame are performed using an initial solution that is either generated by a global-chemistry model or constructed from a known solution at different flow conditions. Occasionally, such calculations are also performed from a cold-flow solution and by using a high-temperature ignition spot. In the present study, calculations for the flame at a given stretch rate are performed from a known solution at a lower stretch rate. Note that this approach resulted in accurate predictions of the double-flame structure for low-stretch-rate cases and the single-flame structure for the high-stretch-rate cases, but failed to predict the single-flame structure for the low-stretch-rate  $204\text{-s}^{-1}$  case. While repeating the calculations for the  $204\text{-s}^{-1}$  case using different initial conditions, accidentally one calculation was provided with a high-stretch-rate flame as initial solution. Surprisingly, that calculation converged

to a single-flame structure – just the way that was seen in the experiments, and gave the first indication for the existence of two stable states for the methane–air/hydrogen–air flame system.

For understanding the double-state behavior of the counterflow premixed flames, experimental and numerical studies are performed on a flame system with  $\Phi_{CH_4} = 0.64$ ,  $\Phi_{H_2} = 0.28$ . Calculations are performed first for a low-stretch-rate case using the global-chemistry solution as the initial data and then for higher-stretch-rate cases using previously obtained solution as the initial data. Calculations are repeated for all the stretch-rate cases starting from the highest-stretched flame and then by decreasing the stretch rate. Peak temperature ( $T_f$ ) along the centerline computed for various stretch rates are shown in Fig. 2. Data computed with increasing-stretch-rate approach are shown with open circles and those computed with decreasing-stretch-rate approach are shown with solid circles. Solid and broken lines are drawn through the symbols for clarity. For all the stretch rates  $\geq 168\text{ s}^{-1}$  flame

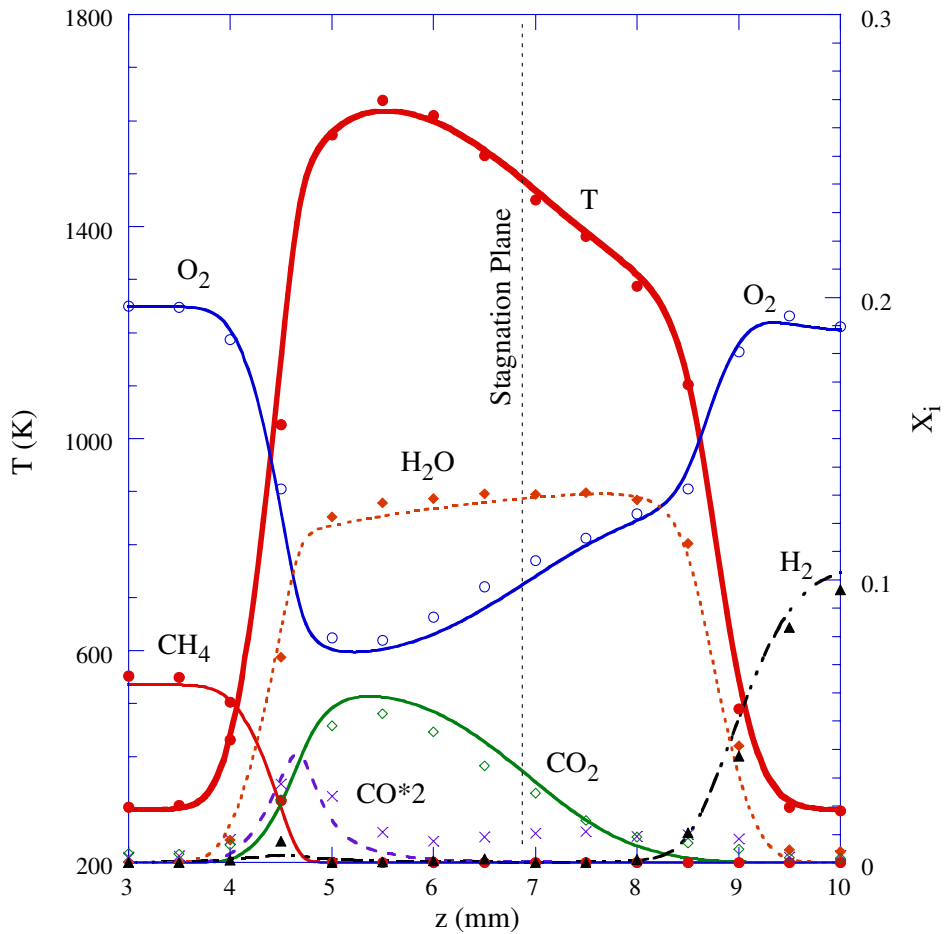


Fig. 3. Computed (lines) and measured (symbols) temperature and species distributions along stagnation line for the flame in State A.  $\Phi_{\text{CH}_4} = 0.64$ ,  $\Phi_{\text{H}_2} = 0.28$ ,  $k_{\text{global}} = 143 \text{ s}^{-1}$  flame.

system has a unique solution independent of how that strain rate was arrived at. There is a slight scatter in the temperature data as the planar flames formed in the counterflow burner tend to oscillate weakly. For all the stretch rates  $< 168 \text{ s}^{-1}$  flame system has two stable states; namely, A and B. Therefore, flame temperature in this regime depends on the way the stretch rate was achieved, i.e., through increasing or decreasing. Note, the double-state behavior is also confirmed with OPPDIF code and using increasing- and decreasing-stretch-rate approaches.

Experiments for the  $\Phi_{\text{CH}_4} = 0.64$ – $\Phi_{\text{H}_2} = 0.28$  flame system at a given stretch rate are performed first by establishing the flame using a blow torch and then significantly perturbing the flame using a metal wire. Inline with the computations, experiments have also shown the existence of two stable states. The two peak temperatures measured for the  $143\text{-s}^{-1}$ -stretch-rate case are shown in Fig. 2 using solid squares. Good agreement between predictions and experiments was found for both

states (A and B). Computed-flame images in terms of temperature distributions corresponding to these states are shown in Fig. 2 as insets. Several observations can be noted from the flame behavior:

1. Transition from state A to B occurs sharply with a small change in stretch rate.
2. Once the flame system is in state B, it is not possible to bring it back to state A through changing stretch rate. State A was achieved through the use of global-chemistry solution as initial condition in the calculations and through the use of flame torch for ignition in the experiment.
3. Peak temperature decreases (from 1722 K) with stretch rate when the flame system is in state A and increases (from 1160 K) when it is in state B.

Detailed comparisons between the predicted and measured structures of the  $143\text{-s}^{-1}$ -stretch-rate

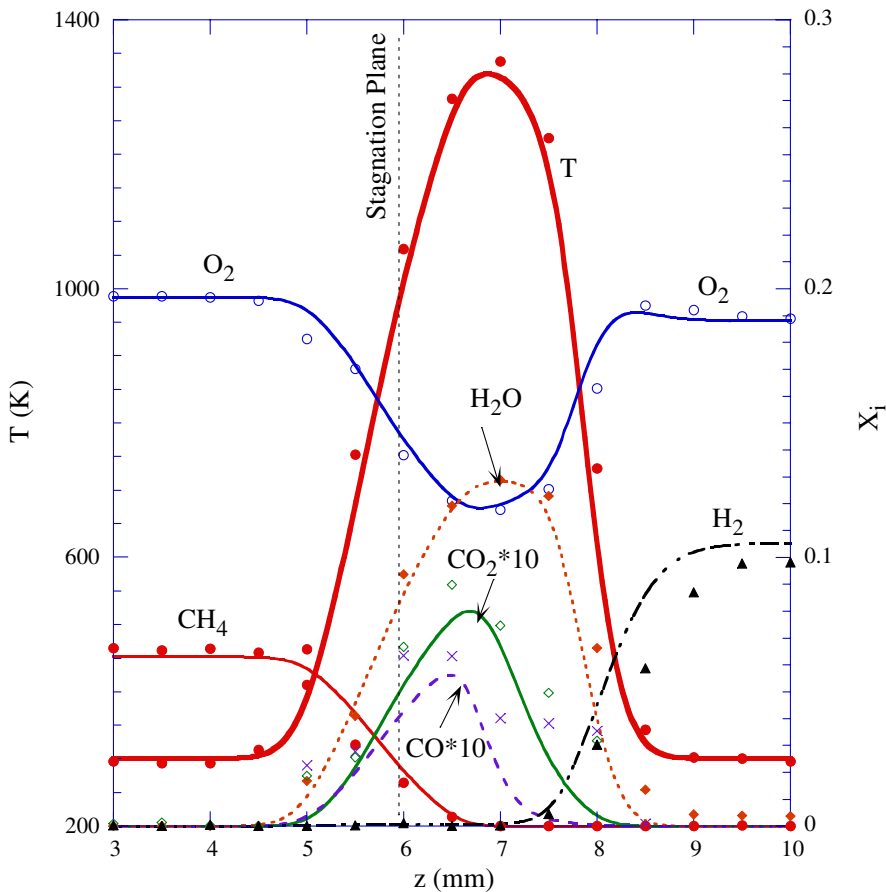


Fig. 4. Computed (lines) and measured (symbols) temperature and species distributions along stagnation line for the flame in State B.  $\Phi_{\text{CH}_4} = 0.64$ ,  $\Phi_{\text{H}_2} = 0.28$ ,  $k_{\text{global}} = 143 \text{ s}^{-1}$  flame.

flame system for states A and B are shown in Figs. 3 and 4, respectively. Temperature and species distributions along the centerline are compared. Here,  $z$  is the distance from the top nozzle. Locations of the stagnation points are indicated with vertical lines. Note that the flow and boundary conditions for the flame systems shown in Figs. 3 and 4 are identical. The only difference between these two flame systems is in the way they were arrived at, i.e., in the initial conditions. The double-flame structure of state A (Fig. 3) is well reproduced. The methane–air mixture produced a flame on the left side ( $z \sim 5.4 \text{ mm}$ ) of the stagnation point with a peak temperature of  $\sim 1720 \text{ K}$  and the hydrogen–air mixture produced a flame on the right side ( $z \sim 8.1 \text{ mm}$ ) with a temperature of  $\sim 1300 \text{ K}$ . When the flame system is operating in state B (Fig. 4), the methane flame extinguished and only the hydrogen flame is established at  $z \sim 7 \text{ mm}$  with a peak temperature of  $\sim 1320 \text{ K}$ . Due to lack of methane combustion only trace amounts of CO and  $\text{CO}_2$  are produced. Complete depletion of methane in Fig. 4 is resulting from the counterflow

geometry rather than from combustion. Over all, very good agreement between experiment and calculations is achieved for the flames in the two different states.

The major distinction between the flames in states A and B is that methane is burning in one state (A) and is not in the other (B). This means that the temperature resulting from hydrogen–air combustion is not sufficient for igniting the methane–air mixture with  $\Phi = 0.64$ . It is known that ignition temperature for fuel-lean mixture decreases with equivalence ratio. Therefore, for a particular equivalence ratio  $> 0.64$  the counterflow premixed flame system may not exhibit double-state behavior. For verifying this hypothesis a series of calculations are performed by using methane–air mixtures with different equivalence ratios. Both the increasing- and decreasing-stretch-rate approaches are used. Equivalence ratio for  $\text{H}_2/\text{air}$  mixture was not changed ( $\Phi_{\text{H}_2} = 0.28$ ).

Computed peak flame temperatures along the centerline for various  $\text{CH}_4/\text{air}$  equivalence ratios

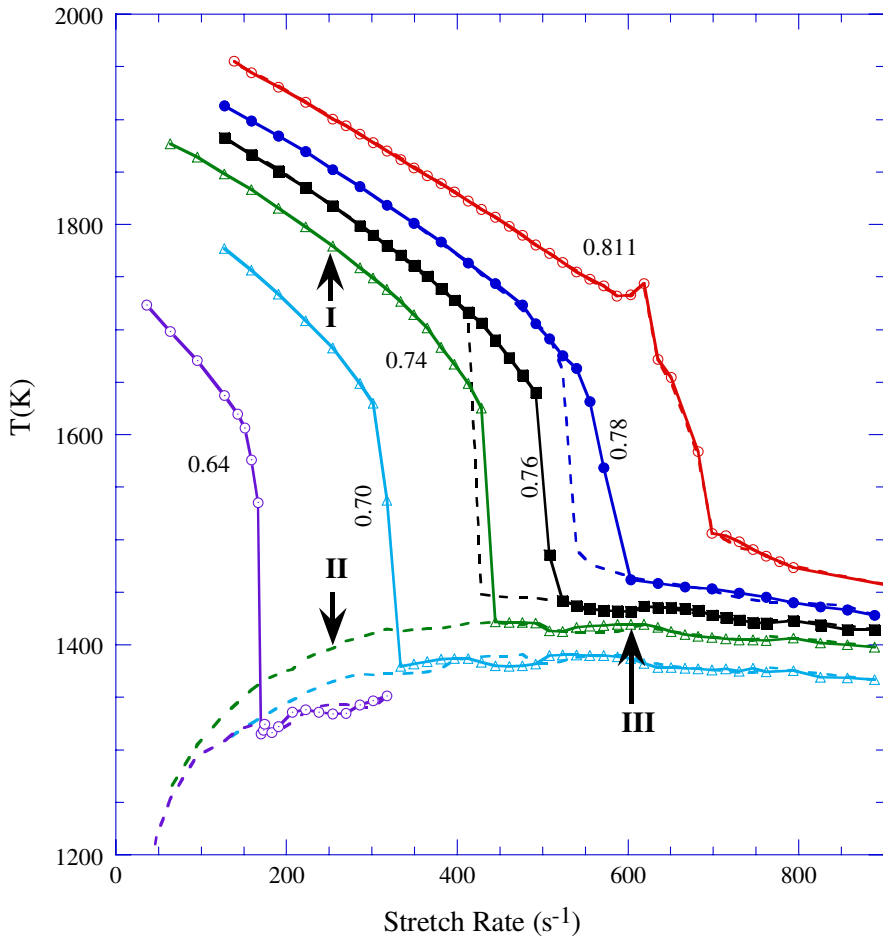


Fig. 5. Response of various premixed flames formed between counter-flowing methane–air and hydrogen–air jets to increasing (symbols) and decreasing (broken lines) strain rates.  $\Phi_{\text{CH}_4}$  is varied while  $\Phi_{\text{H}_2}$  is kept constant at 0.28.

are shown at different stretch rates in Fig. 5. Symbols represent the data obtained while increasing the stretch rate and solid lines are the curves fitted through this data. Broken lines represent the curves passing through the data obtained while decreasing the stretch rate. The transition at which flame system jumps from state A to B is shifted to higher stretch rates as the  $\text{CH}_4/\text{air}$  equivalence ratio is increased. Moreover, transition took place over a wider range of stretch rates in higher  $\text{CH}_4/\text{air}$ -equivalence-ratio cases. Unlike in the case of  $\Phi_{\text{CH}_4} = 0.64$ , where flame system exhibited double-state behavior, the decreasing-stretch-rate data (broken line) for  $\Phi_{\text{CH}_4} = 0.811$  followed the increasing-stretch-rate data (solid line) – suggesting that the flame system did not possess double-state behavior. Nevertheless, the flame system still has a double-flame structure for stretch rates  $< 610 \text{ s}^{-1}$  and a single-flame structure (with methane flame being extinguished) for stretch rates  $> 700 \text{ s}^{-1}$ . More interestingly, for

intermediate  $\text{CH}_4/\text{air}$  equivalence ratios such as 0.76 and 0.78, flame system exhibits hysteresis. For example, in  $\Phi_{\text{CH}_4} = 0.76$  case, flame system stays in state A (double-flame state) until the stretch rate is increased beyond  $500 \text{ s}^{-1}$ , but it does not come back to state A from state B until the stretch rate is decreased to  $430 \text{ s}^{-1}$ . Such a brief hold back in state B could lead to combustion-induced noise if stretch rate on the flame system were cyclically varied as in unsteady counterflow experiments [22,23].

Reasons for the products-supported premixed flames to exhibit double-state behavior can be understood by studying the differences in flow and chemical structures of flame systems formed under different stretch-rate regimes. Flames in regimes marked as I, II, and III in Fig. 5 for  $\text{CH}_4/\text{air}$  equivalence ratio of 0.74 are considered for this purpose. While regimes I and II represent flames in states A and B, respectively, at a stretch rate of  $250 \text{ s}^{-1}$ , regime III represents the flame in

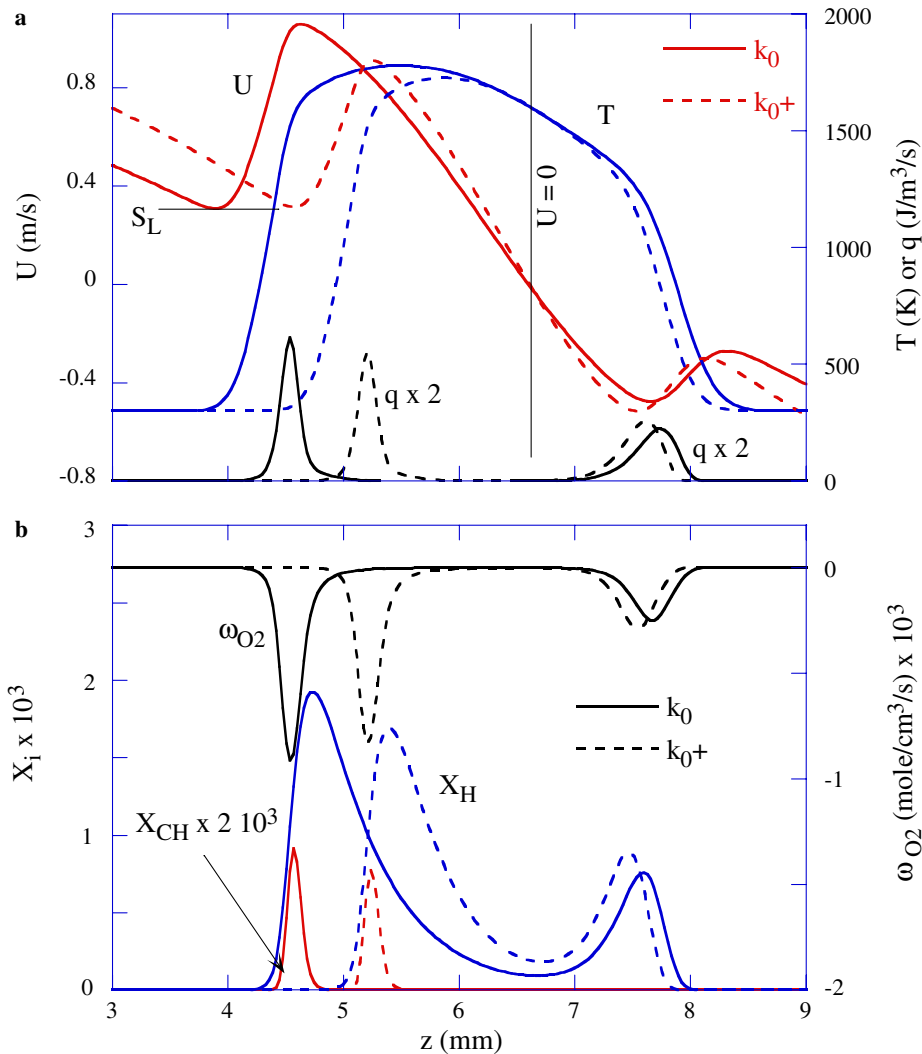


Fig. 6. Changes in flame structure to perturbation in strain rate when State A flame is established under low-strain-rate conditions.  $\Phi_{CH_4} = 0.74$ ,  $\Phi_{H_2} = 0.28$ , and  $k_0 = 250 \text{ s}^{-1}$ . Distributions of (a) velocity, temperature and heat release rate, and (b) H and CH mole fractions and  $O_2$  consumption rate. Broken lines represent the flame structure for  $k_0^+ = 275 \text{ s}^{-1}$ .

state B at a stretch rate of  $600 \text{ s}^{-1}$ . Temperature, velocity, and heat release rate distributions along the centerline for the flames in regimes I, II, and III are shown using solid lines in Figs. 6a, 7a, and 8a, respectively. Concentrations of H and CH radicals and oxygen consumption rates for the three flames are shown using solid lines in Figs. 6b, 7b, and 8b, respectively. Stagnation points are marked with  $U = 0$  lines. Broken lines in Figs. 6–8 represent the data obtained for the flame systems stretched 10% more than those in I, II, and III (i.e.,  $275$ ,  $275$ , and  $660 \text{ s}^{-1}$ ), respectively.

As shown in Fig. 6, both methane and hydrogen flames are present in regime-I flames. Heat

release rate and temperature generated by the methane flame are higher than those generated by the 0.28-equivalence-ratio hydrogen flame. Because of the counterflow configuration heat generated by the hotter methane flame heats the cooler hydrogen flame [24]. Consequently, the temperature of the methane flame is lower and that of the hydrogen flame is higher compared to their respective adiabatic flame temperatures. Note the less-than-unity Lewis number of the hydrogen fuel further increases the flame temperature when the flame is stretched [4]. Heat release rate and oxygen consumption rate indicate that the reaction zones of the two flames are well separated. However, temperature and

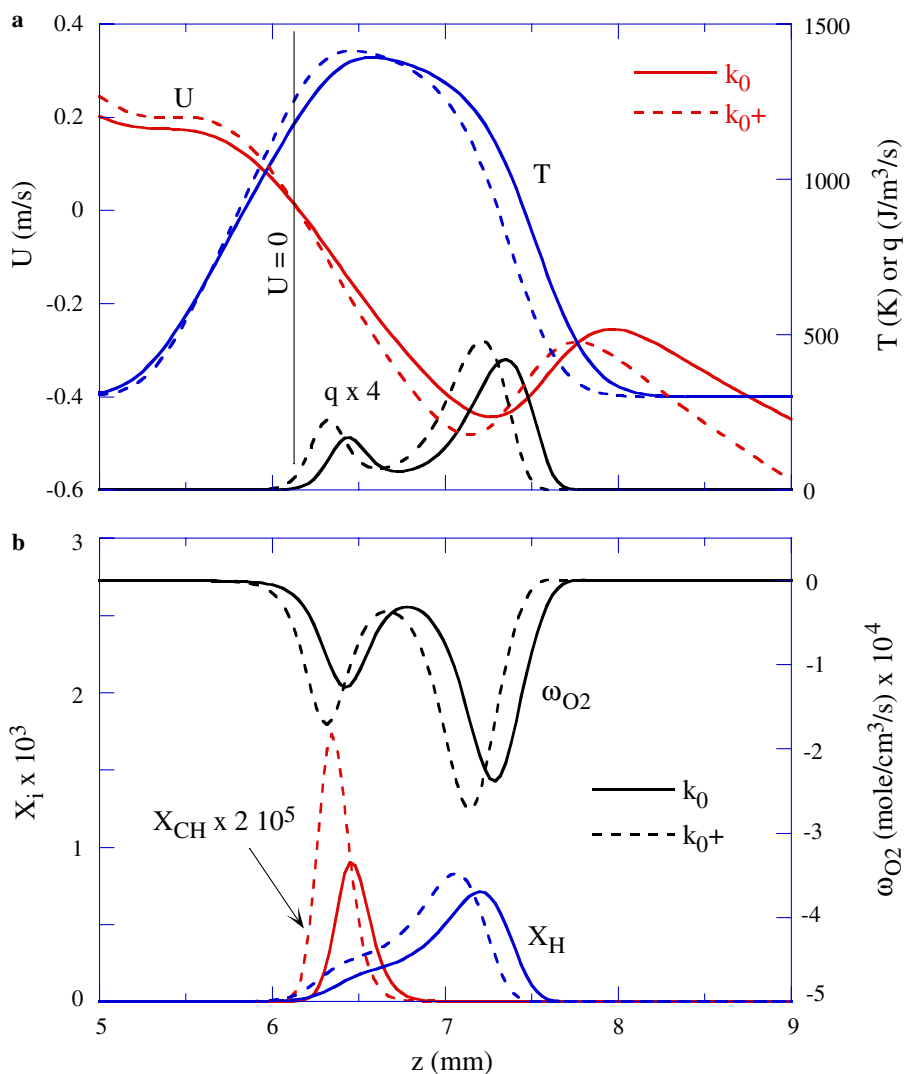


Fig. 7. Changes in flame structure to perturbation in strain rate when State B flame is established under low-strain-rate conditions.  $\Phi_{CH_4} = 0.74$ ,  $\Phi_{H_2} = 0.28$ , and  $k_0 = 250 \text{ s}^{-1}$ . Distributions of (a) velocity, temperature and heat release rate, and (b) H and CH mole fractions and O<sub>2</sub> consumption rate. Broken lines represent the flame structure for  $k_0^+ = 275 \text{ s}^{-1}$ .

H-mole-fraction distributions suggest a strong interaction between the two flames through product species. These flames come closer when the stretch rate on the system increases (compare solid and broken lines in Fig. 6), which results in more interaction between the two flames. As a result, the temperature of the methane flame decreases further and that of hydrogen flame increases further; which, as shown in Figs. 2 and 5, translates into a decrease in peak temperature of the flame system with stretch rate (for regime I flames).

Extinction temperature for hydrogen flames ( $\sim 1150 \text{ K}$ ) [25] is less than that of methane flames ( $\sim 1500 \text{ K}$ ) [26]. As a result, the methane flame extinguishes first when the temperature of the meth-

ane-air/hydrogen-air flame system decreases and the structure of the double-flame system transitions into a single-flame one (regime II) as shown in Fig. 7. Unburned methane gas in this mode diffuses into the products generated by the hydrogen flame and a part of it gets decomposed (low-temperature chemistry) and releases a small amount of heat. Significant drop in oxygen consumption rate and CH and H mole fractions also suggest incomplete combustion of methane fuel. Nevertheless, reaction zones for the two fuels came close to each other and interacting directly. Note the peak in heat release rate from methane decomposition appearing on the hydrogen side of the stagnation point. As diffusion fluxes increase with stretch rate, heat release rate and temperature also increase (compare

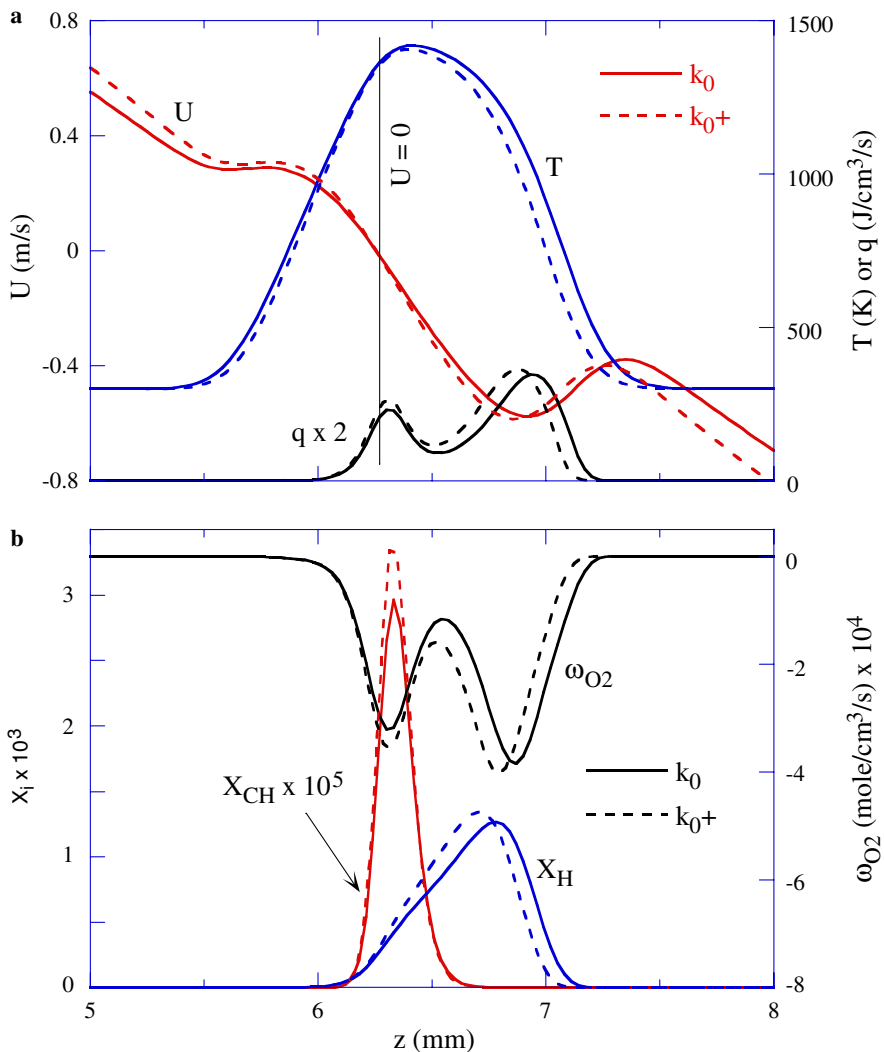


Fig. 8. Changes in flame structure to perturbation in strain rate when flame is established under high-strain-rate conditions.  $\phi_{CH_4} = 0.74$ ,  $\phi_{H_2} = 0.28$ ,  $k_0 = 620 \text{ s}^{-1}$ . Distributions of (a) velocity, temperature and heat release rate, and (b) H and CH mole fractions and  $O_2$  consumption rate. Broken lines represent the flame structure for  $k_0^+ = 660 \text{ s}^{-1}$ .

the solid and broken lines in Fig. 7). This translates into an increase in peak temperature of the flame system with stretch rate (for regime II flames) as shown in Figs. 2 and 5.

Either from regime I or regime II, at higher stretch rates the flame system moves into regime III. Methane fuel diffuses into the products of the hydrogen flame and participates in low-temperature chemistry. According to flamelet theory for non-premixed combustion [27] reaction-zone temperature decreases, even though heat release rate continues to increase, with stretch rate due to reduced reaction-zone thickness and, thereby, increased heat losses (compare solid and broken lines in Fig. 8). This translates into a decrease in peak temperature of the flame system with stretch

rate (for regime III flames) as shown in Figs. 2 and 5.

Double-state behavior of counterflow premixed flames can be explained by considering their characteristics in different regimes (I, II and III). High-energy ignition sources such as a blow torch establish state-A flames with methane and hydrogen burning in regime I. When stretch rate is increased, flame temperature decreases due to aerodynamic heat loss and the flame system transitions to state B when the methane flame extinguishes. Such a transition occurs at relatively low stretch rates in regime II for leaner methane/air mixtures. When stretch rate on a state-B flame with  $\phi_{CH_4} < 0.74$  (regime II) decreases, the flame temperature also decreases due to a drop

in diffusion fluxes. The flame remains in state B as the temperature can not reach the ignition value for the methane–air mixture. Therefore, for leaner methane/air mixtures, the flame system allows two stable states at a given stretch rate and exhibits double-state behavior. When stretch rate on a moderately lean state-A flame ( $\phi_{\text{CH}_4} > 0.74$ ) increases it transitions into state B in regime III. If stretch rate of this state-B flame is decreased, then flame temperature increases due to drop in stretch-induced cooling (flamelet description) and the flame system transitions to state A when flame temperature reaches its ignition value. For these equivalence ratios, the flame system does not exhibit double-state behavior.

## 5. Conclusions

The counterflow flame system established between lean-methane–air and lean-hydrogen–air streams was investigated experimentally and numerically. A two-dimensional model known as UNICORN was used for the simulation. GRI version 1.2 chemical kinetics involving 32 species and 346 one-way elementary reactions was used. Detailed measurements for temperature and species concentrations were obtained along the centerline using Raman spectroscopy. A double-state behavior for this flame system was first identified in the numerical simulations, which was later confirmed by the experiments. A good agreement between measurements and calculations was obtained for the flame in different states.

Calculations for various lean methane–air mixtures were performed to understand the double-state behavior of the counterflow premixed flames. Aerodynamic and chemical structures of the flames at different stretch rates were obtained through increasing-stretch-rate and decreasing-stretch-rate approaches. It was found that flame system exhibits double-state behavior only for leaner ( $\phi_{\text{CH}_4} < 0.74$ ) methane–air mixtures. When stretch rate is increased, the flame transitions from a double-flame to a single-flame structure due to aerodynamic cooling. When stretch rate is decreased, the flame does not transition back to the double-flame structure due to stretch effects on molecular diffusion. However, for  $\phi_{\text{CH}_4} > 0.74$ , decrease in stretch rate increases flame temperature due to a decrease in stretch-induced cooling and returns the flame structure to a double-flame one. For a narrow range of equivalence ratios (0.74–0.81) counterflow premixed flames exhibited a hysteresis property.

## Acknowledgments

Financial support for the computational work was provided by the Air Force Office of Scientific

Research (AFOSR, Julian Tishkoff) and the Air Force Contract #F33615-00-C-2068 (Vince Belovich). Financial support for the experimental work was provided by the National Science Foundation (Grant No. CTS-0314704).

## References

- [1] D.C. Haworth, R.J. Blint, B. Cuenot, T.J. Poinot, *Combust. Flame* 121 (3) (2000) 395–417.
- [2] S.H. Sohrab, Z.Y. Ye, C.K. Law, *Proc. Combust. Inst.* 20 (1985) 1957–1965.
- [3] C.K. Law, *Proc. Combust. Inst.* 22 (1988) 1381–1402.
- [4] D.M. Mosbacher, J.A. Wehrmeyer, R.W. Pitz, C.J. Sung, J.L. Byrd, *Proc. Combust. Inst.* 29 (2002) 1479–1486.
- [5] M.A. Tanoff, M.D. Smooke, R.J. Osborne, T.M. Brown, R.W. Pitz, *Proc. Combust. Inst.* 26 (1996) 1121–1128.
- [6] R.S. Barlow, A.N. Karpetis, J.H. Frank, J.-Y. Chen, *Combust. Flame* 127 (2001) 2102–2118.
- [7] J.A. Wehrmeyer, Z. Cheng, D.M. Mosbacher, R.W. Pitz, R. Osborne, *Combust. Flame* 128 (3) (2002) 232–241.
- [8] Z. Cheng, J.A. Wehrmeyer, R.W. Pitz, in: 38th AIAA/ASME/SAE/ASEE Joint Propulsion Conference, AIAA 2002-4021, Indianapolis, IN, 2002.
- [9] N. Darabiha, S.M. Candel, V. Giovangigli, M.D. Smooke, *Combust. Sci. Technol.* 60 (1988) 267–284.
- [10] C.J. Sung, J.B. Liu, C.K. Law, *Combust. Flame* 106 (1–2) (1996) 168–183.
- [11] C.K. Law, C.J. Sung, G. Yu, R.L. Axelbaum, *Combust. Flame* 98 (1–2) (1994) 139–154.
- [12] C.J. Sung, G.J.B. Liu, C.K. Law, *Combust. Flame* 102 (4) (1995) 481–492.
- [13] W.M. Roquemore, V.R. Katta, *J. Visualizat.* 2 (2000) 257–272.
- [14] V.R. Katta, W.M. Roquemore, *Combust. Flame* 100 (1) (1995) 61.
- [15] G.P. Smith, D.M. Golden, M. Frenklach, et al., 2001, available at <http://www.me.berkeley.edu/gri-mech>.
- [16] Annon., Computational Submodels, International Workshop on Measurement and Computation of Turbulent Nonpremixed Flames. Available at <http://www.ca.sandia.gov/TNF/radiation.html>.
- [17] V.R. Katta, L.P. Goss, W.M. Roquemore, *AIAA J.* 32 (1) (1994) 84.
- [18] V.R. Katta, L.P. Goss, W.M. Roquemore, *Int. J. Num. Meth. Heat Fluid Flow* 4 (5) (1994) 413.
- [19] K. Seshadri, I. Puri, N. Peters, *Combust. Flame* 61 (3) (1985) 237–249.
- [20] Z. Cheng, J.A. Wehrmeyer, R.W. Pitz, *Proc. Combust. Inst.* 30 (2005) 285–293.
- [21] V.R. Katta, Z. Cheng, R.W. Pitz, in: Proceedings of the 4th Joint Meeting of the US Sections of the Combustion Institute, Philadelphia, PA, 21–23 March 2005.
- [22] H.G. Im, C.K. Law, J.S. Kim, F.A. Williams, *Combust. Flame* 100 (1995) 21–30.
- [23] F.N. Egolfopoulos, C.S. Campbell, *J. Fluid Mech.* 318 (1996) 1–29.
- [24] C.J. Sung, C.K. Law, AIAA Paper, presented at the Aerospace Sciences Meeting and Exhibit, Reno, NV, 12–16 January 1993.

- [25] V.R. Katta, T.R. Meyer, M.S. Brown, J.R. Gord, W.M. Roquemore, *Combust. Flame* 137 (2004) 198–221.
- [26] V.R. Katta, W.M. Roquemore, *Extinction in Methane–air Counterflow Diffusion Flame—A Direct*

*Numerical Study*, Central States section Meeting of the Combustion Institute, St. Louis, Paper No. 80, 1996, pp. 449–454.

- [27] N. Peters, *Proc. Combust. Inst.* 21 (1986) 1231–1256.

## Comment

*Vadim Kurdioumov, CIEMAT, Spain.* Is it possible to obtain a similar effect in the flame of the one-dimensional model of the counter-flow?

*Reply.* The double-state behavior of the premixed flame system is resulting from the heat and mass transport responses to the changes in applied strain rate. However, as this behavior is triggered by the flame (methane) extinction process, accurate modeling of not only the heat and mass transports but also the chemical kinetics is essential for its prediction. Our two-dimensional, time-dependent model (UNICORN) accurately simulated the counterflow experiment and, hence, predicted the double-state behavior. In an unpublished effort, we made several attempts to simulate the double-state behavior of the flame system using OPPDIF, a

steady one-dimensional model. Using OPPDIF, the double-state behavior was found when GRI Version 2.11 mechanism with multicomponent formulation for transport (using mixture-averaged transport failed) was used, while attempts using other chemical kinetic mechanisms (GRI Version 3.0, San Diego) failed to predict the double-state behavior using either multicomponent or mixture-averaged molecular transport model. The successful OPPDIF prediction of State B had a peak temperature of 1400 K compared to the UNICORN prediction of 1315 K (1340 K  $\pm$  40 K was measured). Further efforts using the UNICORN code with different chemical kinetic mechanisms and transport models would help to make a definite conclusion about whether accurate and reliable prediction of these double states requires a two-dimensional model.